JOURNAL OF COMPUTATIONAL PHYSICS 20, 33–49 (1976)

On the Use of a Scale-Dependent Filter in Channel Model Integrations

STEPHEN MUDRICK

Air Force Cambridge Research Laboratories, Hanscom Air Force Base, Massachusetts 01731

Received April 18, 1975; revised June 24, 1975

A channel model using a finite-difference gridpoint method is described. Integrations with this model produce large amplitude, high wavenumber "noise" near the lateral walls, which corrupts the interior solution. A technique is presented that employs scale-dependent filters to eliminate the generation of the boundary noise, while leaving the interior flow relatively unchanged. The effectiveness of the technique is demonstrated.

1. INTRODUCTION

This paper describes some work done with a primitive equation model and with a scale-dependent filtering technique [10]. As part of his Doctoral research at the Massachusetts Institute of Technology, the author intended to use this model to study the growth of and subsequent frontogenesis associated with unstable Eady waves (see, for example, [1]) in a channel flow. Such integrations could not be completed because of short wavelength, large amplitude waves, which developed at the channel walls and dominated the interior flow evolution. This lateral boundary problem was never overcome; instead, a different basic state modeling an internal, baroclinic jet in a channel was chosen for study. Near the lateral walls, the wind was reduced to zero so the evolving flow was never affected by the boundary problem. The resulting work is described by Mudrick [5, 6].

This difficulty with boundary "noise" certainly is not confined to the Eady wave within channel flow problem. Hunt [3] experienced a similar problem with his "semi-spectral" global atmospheric integrations, and he chose a filter similar to the technique discussed here.

The above-mentioned works used inviscid equations with appropriate boundary conditions. The difficulty may arise ultimately because of the lack of viscous effects in the model flows. As discussed by Gal-Chen and Somerville [2], a flow containing viscosity, no matter how small, will always form viscous boundary layers near physical boundaries. These layers confine wall effects to the region near the walls. One might try to match a boundary layer solution for viscous, near-wall flow to the

assumed inviscid flow outside the boundary layer; this not only is a difficult fluid dynamics problem but also would be expensive from a computational viewpoint. We prefer to maintain the simpler inviscid model formulation.

The use of filtering to prevent boundary effects from corrupting the interior flow is not new. The purpose of this paper is to demonstrate the ability of Shapiro's [9, 10] scale-dependent filtering technique to perform this task. The filter described here is only a numerical procedure applied with no physical models in mind, yet it works in a manner similar to a viscous boundary layer by insulating the interior flow from wall effects.

2. The Model

The basic set of nondimensional equations is for a dry, hydrostatic, inviscid, adiabatic atmosphere. The Boussinesq approximation is made. The domain of integration is a reentrant channel with rigid horizontal and vertical boundaries: $0 \leqslant x \leqslant l$, $0 \leqslant y \leqslant 1$, $0 \leqslant z \leqslant 1$, and $0 \leqslant t$, where l is the nondimensional channel length. The equations are

$$\frac{du}{dt} - fv = -\frac{\partial p}{\partial x}$$

$$\frac{dv}{dt} + fu = -\frac{\partial p}{\partial y}$$

$$\frac{db}{dt} = 0$$

$$b = \frac{\partial p}{\partial z}$$

$$\frac{\partial u}{\partial x} + \frac{\partial v}{\partial y} + \frac{\partial w}{\partial z} = 0$$

where

$$\frac{d}{dt} = \frac{\partial}{\partial t} + u\frac{\partial}{\partial x} + v\frac{\partial}{\partial y} + w\frac{\partial}{\partial z}.$$

The boundary conditions are

$$w(x, y, 0) = w(x, y, 1) = v(x, 0, z) = v(x, 1, z) = 0; \quad \alpha(x \pm l, y, z) = \alpha(x, y, z),$$

where α is any variable. In these integrations the Coriolis parameter f is constant and equal to unity. The variable b is called the "buoyancy."

These equations are integrated in time by a two step, Lax–Wendroff-like

procedure using a staggered Eliassen grid representation of the variables. It is an extension to three space dimensions of the two-dimensional scheme of Phillips [7] and is of second-order accuracy in space and time with respect to truncation error. Since the above reference is somewhat obscure, a brief explanation of the scheme, closely following [7], is given for the variable u. Variables v and b are similar.

Consider the x component of the equation of motion written symbolically as $du/dt = X$, where X represents the x component of force. Let the variables be known at time $t = n\,\Delta t$, the nth timestep. The first step of the procedure is to calculate u at the half timestep $(n + \frac{1}{2})\,\Delta t$, from values of the variables at time $n\,\Delta t$, by doing an upstream trajectory calculation directly for du/dt. Allowing a prime to indicate a half timestep quantity, we write the above equation as

$$u'[x, y, z, (n + \tfrac{1}{2})\,\Delta t] = u^*(x^*, y^*, z^*, n\,\Delta t) + \tfrac{1}{2}\,\Delta t\, X_{x,y,z,n\Delta t},$$

where the subscript means X is evaluated from variables at that place and time. The variable u^* is the value of u at time $n\,\Delta t$ at the point

$$x^* = x - \tfrac{1}{2}\bar{u}\,\Delta t, \qquad y^* = y - \tfrac{1}{2}\bar{v}\,\Delta t, \qquad z^* = z - \tfrac{1}{2}\bar{w}\,\Delta t,$$

where $\bar{u}$, $\bar{v}$, and $\bar{w}$ are suitably averaged values of u, v, and w in the neighborhood of point (x, y, z), at time $n\,\Delta t$. (Due to the staggered grid, x, y, and z will have differing values depending upon the variable being forecast.) Thus, the point (x^*, y^*, z^*) defines the location at time $n\,\Delta t$ of the particle which at time $(n + \frac{1}{2})\,\Delta t$ is located at (x, y, z). Then $2(u' - u^*)/\Delta t$ is a direct, "uncentered" finite-difference equivalent to du/dt. Since (x^*, y^*, z^*) normally will not coincide with a gridpoint, u^* must be interpolated from gridpoint values of u at time $n\,\Delta t$. The interpolation formulas are discussed for the two-dimensional case in [7], as are the formulas for $\bar{u}$ and $\bar{v}$ mentioned above.

At the full timestep $(n + 1)\,\Delta t$, centered differences in time are used with the advective terms in "flux" or conservation law form:

$$u[x, y, z, (n + 1)\,\Delta t]$$

$$= u(x, y, z, n\,\Delta t) + \Delta t \left(-\frac{\partial}{\partial x} u'u' - \frac{\partial}{\partial y} v'u' - \frac{\partial}{\partial z} w'u' + X'\right)_{x,y,z,(n+(1/2))\,\Delta t}.$$

The half timestep procedure used above damps slightly all wavelengths greater than two grid intervals, short waves more so than longer waves. The staggered grids (described below) vary in position at the half and full timesteps. The variables p and w are calculated diagnostically from the hydrostatic and continuity equations, respectively, both at the half and full timesteps, subsequent to the forecasts of b, u, and v; p is on the same vertical level as are b, u, and v while w is staggered between them in the vertical.

We now describe the staggered location of the variables on the discrete grid. Primed variables refer to the half timestep $(n + \frac{1}{2})\,\Delta t$, and unprimed variables refer to the full timestep $(n + 1)\,\Delta t$, for the nth timestep. Let the indices i, j, k represent the discretized location of the variables with respect to the x, y, z coordinate system. We have $i = 1, 2, \ldots, I$; $j = 1, 2, \ldots, J - 1$ or J as described below; and $k = 1, 2, \ldots, K$. The lowest level is at $k = 1$. Further, let $\Delta x = l/(I - 2)$, $\Delta y = 1/(J - 2)$, and $\Delta z = 1/K$.

At the half timestep the locations of the variables are as follows:

b'_{ijk}, p'_{ijk}	$x = (i - 1)\Delta x$,	$y = (j - 1)\Delta y$,	$z = (k - 1/2)\Delta z$,	$j\max = J - 1$
u'_{ijk}	$x = (i - 1)\Delta x$,	$y = (j - 3/2)\Delta y$,	$z = (k - 1/2)\Delta z$,	$j\max = J$
v'_{ijk}	$x = (i - 1/2)\Delta x$,	$y = (j - 1)\Delta y$,	$z = (k - 1/2)\Delta z$,	$j\max = J - 1$
w'_{ijk}	$x = (i - 1/2)\Delta x$,	$y = (j - 3/2)\Delta y$,	$z = k\,\Delta z$,	$j\max = J$.

At the full timestep, we have:

b_{ijk}, p_{ijk}	$x = (i - 1/2)\Delta x$,	$y = (j - 3/2)\Delta y$,	$z = (k - 1/2)\Delta z$,	$j\max = J$
u_{ijk}	$x = (i - 1/2)\Delta x$,	$y = (j - 1)\Delta y$,	$z = (k - 1/2)\Delta z$,	$j\max = J - 1$
v_{ijk}	$x = (i - 1)\Delta x$,	$y = (j - 3/2)\Delta y$,	$z = (k - 1/2)\Delta z$,	$j\max = J$
w_{ijk}	$x = (i - 1)\Delta x$,	$y = (j - 1)\Delta y$,	$z = k\,\Delta z$,	$j\max = J - 1$.

The above arrangement is summarized in Fig. 1.

The periodic boundary conditions in the x direction are included on the discrete grid as follows. Let α_{ijk} be any variable on the grid; α_{ijk} for $i = 2$ to $I - 1$ is computed from the appropriate equation. Then $\alpha_{1jk} = \alpha_{I-1,j,k}$ and $\alpha_{Ijk} = \alpha_{2jk}$.

The lateral boundary conditions at the $y = 0$ wall will now be discussed; the boundary conditions at the $y = 1$ wall are similar. (For convenience, we shall refer to the $y = 0$ wall as the "southern" wall and to the $y = 1$ wall as the "northern" wall, as if the channel is aligned east–west.)

At the half timestep: b'_{i1k} and v'_{i1k} lie within the domain $(0 \leqslant y \leqslant 1)$ while u'_{i1k} and w'_{i1k} lie $\Delta y/2$ outside the domain and, hence, must be computed diagnostically from values inside the domain. We require: b'_{i1k}, forecast as are interior values of b'_{ijk}; u'_{i1k}, computed from interior values of u'_{ijk}, v'_{ijk} by requiring that the relative vorticity $\partial v/\partial x - \partial u/\partial y$ be the same on the boundary as at the first interior row; $v'_{i1k} = 0$; and $w'_{i1k} = w'_{i2k}$.

At the full timestep: u_{i1k} and w_{i1k} lie within the domain $(0 \leqslant y \leqslant 1)$ while b_{i1k} and v_{i1k} lie $\Delta y/2$ outside the domain and, hence, they must be computed diagnostically from values inside the domain. We require: b_{i1k}, computed from interior values of u_{ijk}, b_{ijk} from the thermal wind relation $\partial b/\partial y = -f(\partial u/\partial z)$, which is

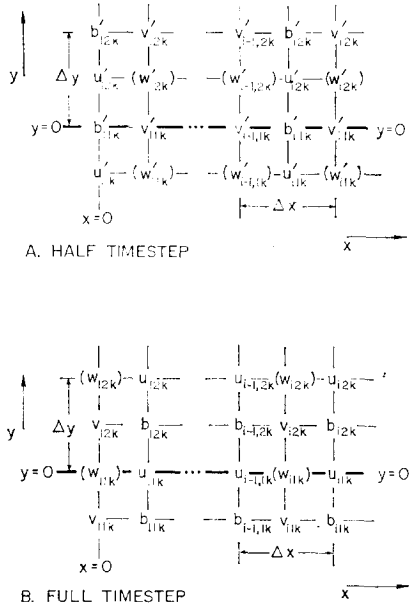

FIG. 1. Arrangement of variables near $y = 0$ (southern wall) for $x - y$ plane at level $z = \Delta z(k - \frac{1}{2})$. Variables in parentheses are located $\frac{1}{2}\Delta z$ above this level. Both p'_{ijk} and p_{ijk} are at same locations as are b'_{ijk} and b_{ijk}, respectively.

exact at $y = 0$ since $v = 0$ (see Appendix 2 for additional details); u_{i1k}, forecast as are interior values of u_{ijk}; $v_{i1k} = -v_{i2k}$; and w_{i1k}, computed as are interior values of w_{ijk}.

Various changes were made in the boundary conditions, all second-order accurate in space, but no improvement in model performance was effected with respect to the lateral boundary problem. Mudrick [5] provides more details concerning the model equations and finite-difference techniques.

It was noticed that for the Eady cyclogenesis case as described below (both in integrations at the Massachusetts Institute of Technology and AFCRL), regions of negative buoyancy lapse rate tended to develop near the lateral boundaries. Within these regions, $\Delta b/\Delta z$ became negative, corresponding to superadiabatic atmospheric lapse rates. These were generated by unrealistic values of b associated with the high wavenumber "noise" at the lateral boundaries.

A dry, convective adjustment scheme similar to that of Manabe *et al.* [4] therefore was added to the model. A column undergoing adjustment has $\Delta b/\Delta z$ set to zero from its negative value; potential energy of the column is conserved during adjustment. This procedure will decrease the average buoyancy of the column so total buoyancy no longer will be conserved during an integration but

will decrease with time (see Appendix 1). As the lateral boundary noise develops much earlier in the runs than do the areas of negative buoyancy lapse rate, inclusion of the convective adjustment scheme will not alleviate this problem, but convective adjustment will eliminate the danger of further generation of high wavenumber components by "gravitational instability."

3. The Filter

As mentioned, the finite-difference scheme contains implicit damping of short waves. This damping is not sufficient to reduce the high wavenumber components being generated at the lateral boundaries. The addition of any explicit filter will introduce added dissipation and a loss of energy with time. We wish to confine this loss to the higher wavenumber noise. A filter will be considered to be "effective" if it can remove the noise generated mainly at the boundaries and yet leave relatively unchanged the amplitude and phase speed of longer waves.

Shapiro [9, 10] has developed a class of linear filters that can be made increasingly scale dependent; as the order of the filter is increased, it becomes more sensitive in its discrimination between long and short wave components. Such a filter removes two-grid interval waves completely, yet can produce little or no damping of longer waves (see [10, Table 1], for example).

The specific filter used here is based upon the stencils presented by Shapiro's [10, Table 2] and is applied to the channel model, after each full timestep computation, as follows. (His Table 2, modified slightly, is presented herein as Table I.) The prognostic variables b_{ijk}, u_{ijk}, and v_{ijk} are filtered; the diagnostic fields p_{ijk} and w_{ijk} are not.

A "symmetric" filter is used; that is, the same order filter that is applied east–west is applied north–south, starting with row $j = 2$ which is just inside the southern wall (see Fig. 1).

The filter is applied in two passes. First a north–south filter is used, starting with row $j = 2$. For this row, we use what Shapiro calls the "zero-order" filter

$$\tilde{\alpha}_{i2k} = \tfrac{1}{4}(\alpha_{i1k} + 2\alpha_{i2k} + \alpha_{i3k}),$$

where α_{ijk} is a variable at the i, j, k gridpoint. For row $j = 3$, we use the "first-order" filter

$$\tilde{\alpha}_{i3k} = \tfrac{1}{16}(-\alpha_{i1k} + 4\alpha_{i2k} + 10\alpha_{i3k} + 4\alpha_{i4k} - \alpha_{i5k}).$$

As we go further into the interior (increasing j) we increase the order of the filter until at row $j = 7$, and for the remainder of the interior we use a "fifth-order" filter (see Table I; replace m by j). The same procedure is used near the northern wall.

TABLE I

Filter Stencil for Various Orders p[a]

p		m	$m \pm 1$	$m \pm 2$	$m \pm 3$	$m \pm 4$	$m \pm 5$	$m \pm 6$	$m \pm 7$	$m \pm 8$	$m \pm 9$	$m \pm 10$
0	$1/2^2$	(2	1)									
1	$1/2^4$	(10	4	−1)								
2	$1/2^6$	(44	15	−6	1)							
3	$1/2^8$	(186	56	−28	8	−1)						
4	$1/2^{10}$	(772	210	−120	45	−10	1)					
5	$1/2^{12}$	(3,172	792	−495	220	−66	12	−1)				
6	$1/2^{14}$	(12,952	3,003	−2,002	1,001	−364	91	−14	1)			
7	$1/2^{16}$	(52,666	11,440	−8,008	4,368	−1,820	560	−120	16	−1)		
8	$1/2^{18}$	(213,524	43,758	−31,824	18,564	−8,568	3,060	−816	153	−18	1)	
9	$1/2^{20}$	(863,820	167,960	−125,970	77,520	−38,760	15,504	−4,845	1,140	−190	20	−1)

[a] The m represents an i or a j, depending upon whether the variable α_{ijk} is being filtered in the east–west or in the north–south direction, respectively.

No filtering is done on row $j = 1$, which falls outside the boundary for b_{i1k} and v_{i1k} and on the boundary for u_{i1k}, and no filtering is done in the vertical.

Next, an east–west filter is applied to the $\tilde{\alpha}_{ijk}$ field, starting again at row $j = 2$ and proceeding into the interior:

$$\tilde{\tilde{\alpha}}_{i2k} = \tfrac{1}{4}(\tilde{\alpha}_{i-1,2k} + 2\tilde{\alpha}_{i2k} + \tilde{\alpha}_{i+1,2k}),$$

$$\tilde{\tilde{\alpha}}_{i3k} = \tfrac{1}{16}(-\tilde{\alpha}_{i-2,3k} + 4\tilde{\alpha}_{i-1,3k} + 10\tilde{\alpha}_{i3k} + 4\tilde{\alpha}_{i+1,3k} - \tilde{\alpha}_{i+2,3k}), \text{ etc.}$$

Again the fifth-order east–west filter is used for rows $j \geqslant 7$ (replace m by i in Table I), and again the same procedure is used near the northern wall. The $\tilde{\tilde{\alpha}}_{ijk}$ field is the fully filtered field.

The construction of this filter is constrained by the fact that the variables are defined for only one row outside the lateral walls. The use of higher-order filters near the walls can be accomplished if approrpiate boundary conditions are present For example, periodic boundary conditions allow any order filter to be extended to all points. One must be careful in defining added boundary values to fit the order of the filter desired; Shapiro [8] describes some disastrous consequences of this approach.

4. The Experiment

The Eady cyclogenesis problem was chosen for experimentation because of its simple basic state and because of the strong vertical wind shear at the lateral boundaries, which leads to the boundary difficulties.

The initial fields of b, u, and v are obtained from the basic state plus a small perturbation. We first describe the basic state. For this experiment, dimensional parameters are taken as follows: The Coriolis parameter f is 10^{-4} sec^{-1}, channel length and width L are 5×10^6 m and depth is 10^4 m. The initial atmospheric stability, taken as constant, is obtained by assuming a lapse rate of -6.5°C km^{-1} with a temperature of 265°K at 650 mb. The wind u is a function of height only, varying linearly from 25 m sec^{-1} at the top of the channel to -25 m sec^{-1} at the bottom; the vertically averaged wind is thus zero so a growing disturbance will tend to remain fixed in location. The basic state wind components v and w are zero. The above parameters yield a Richardson number of 5.2.

The nondimensional basic state wind is given by $u = 0.10\ (z - \frac{1}{2})$. (Multiply this by $fL = 500$ m sec^{-1} to obtain the dimensional wind.) The wind is balanced geostrophically by a buoyancy field increasing linearly with height and decreasing linearly northward (with increasing y).

The perturbation structure, added to the basic state, is that of an unstable Eady wave in a channel. The maximum value of the perturbation north–south

TABLE II

Percentage Change from Start of Total Energy E and Total Buoyancy B; Actual Value of Total Momentum M

	Run 1			Run 2 *CA*			Run 3 *F*			Run 4 *CA,F*		
Time step	E (%)[c]	B[a] (%)	M[b] (actual value)	E (%)	B (%)	M (actual value)	E (%)	B (%$\times 10^{-6}$)	M (actual value $\times 10^{-9}$)	E (%)	B (%)	M (actual value $\times 10^{-9}$)
20	0.004	0	0				−0.015	−1.76	2.1			
40	0.009	0	0		Same as		−0.052	−2.71	3.2		Same as	
60	0.019	0	0		run 1		−0.126	−3.52	1.9		run 3	
80	0.039	0	0		through		−0.283	−2.44	3.2		through	
100	0.084	0	0		step 120		−0.635	−2.98	2.1		step 160	
120	0.193	0	0				−1.47	−2.30	−1.5			
140	0.474	0	0	0.466	−0.005	0	−3.37	1.35	−6.6			
160	1.15	0	0	1.09	−0.016	0	−7.58	6.10	−19.4			
180	2.44	0	0	2.56	−0.068	0	−15.9	10.2	−31.5	−15.9	−0.002	−38.8
200	6.39	0	0	7.67	−0.257	0	−26.8	30.9	−2.7	−26.8	−0.042	−243.0
220	19.6	0	0	19.6	−0.774	0	−31.9	14.6	106.0	−30.7	−0.235	101.0

CA = convective adjustment; *F* = filter.

[a] A zero in buoyancy column means no percentage change in this quantity to eight decimal places.

[b] Since total momentum is zero to ten decimal places at start, actual values of M are shown for each timestep. A zero in the momentum column means no change in this quantity to ten decimal places.

[c] Percentage change in quantity from value at start of run.

wind v is 5% of the maximum value of the basic state wind. This gives the total wind field. An initialization procedure, described in [5], is then used to obtain adjusted initial wind and buoyancy fields. The initial fields of b, u, and v thus consist of a "basic state" part plus a small perturbation, with some slight modification due to the initialization process. The model now is integrated forward in time; the entire fields of wind and buoyancy are free to evolve.

Four integrations were made on the CDC 6600 at AFCRL: run 1 without convective adjustment and without filtering, run 2 with convective adjustment but no filtering, and runs 3 and 4 without and with convective adjustment, respectively, and both with filtering. The filtering process was applied once each timestep. All runs made had $18 \times 18 \times 5$ gridpoints within the domain of integration, or a dimensional spacing of 278 km in the horizontal and 2 km in the vertical. This resolution allowed for wavenumbers one through nine, wavenumber nine being the two-grid interval wave. A timestep of 0.18 or 30 min was used although the linear stability criterion allowed a maximum step of over 60 min. Runs 1 and 2 were quite similar to each other, as were runs 3 and 4. The major differences resulted from use of the filter rather than from use of the convective adjustment scheme (see Table II and Appendix 1).

5. Results

We now compare the buoyancy field generated by run 2, without filtering, to that generated by run 4, with filtering. Both runs included convective adjustment. (Appendix 1 presents a discussion of these runs and of those without convective adjustment, runs 1 and 3, with respect to the variation of total momentum, buoyancy, and energy.)

The surface buoyancy field (level $k = 1$) at the start of the integration (not shown), decreases linearly northward from a maximum value of 0.106 at the southernmost row to a value of zero at the northernmost row. There is a slight variation in the east–west direction. As the unstable Eady wave amplifies with time, the surface buoyancy field becomes progressively distorted by the northward advection of high b values (warm air) and by the southward advection of low b values (cold air). The "warm tongue" gradually narrows with time as the wave "occludes."

Figures 2 and 3 show the surface buoyancy field at timestep 200 for runs 2 and 4, respectively. We discuss the fields at step 200 because beyond this time, gradients associated with the formation of frontal zones become too narrow to be resolved by the grid spacing. The width of the warm tongue in Figs. 2 and 3 is approaching one grid distance; evidence of truncation error can be seen in the separation of the area warmer than 0.085 into three regions within the warm tongue.

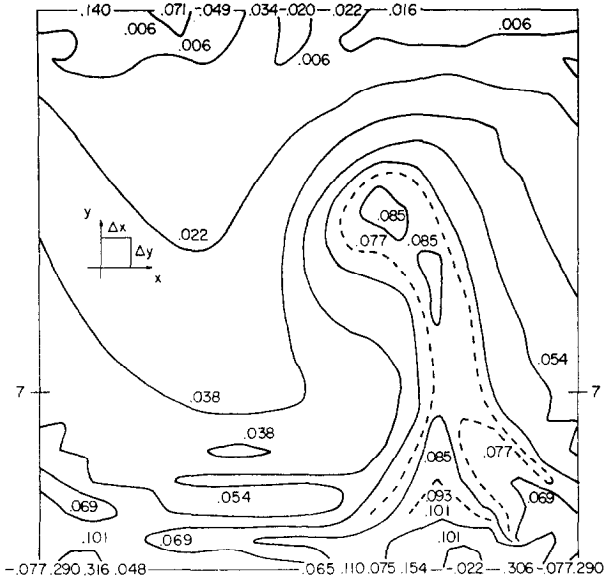

FIG. 2. Surface buoyancy b (level $k = 1$) timestep 200, for run 2, convective adjustment, no filter.

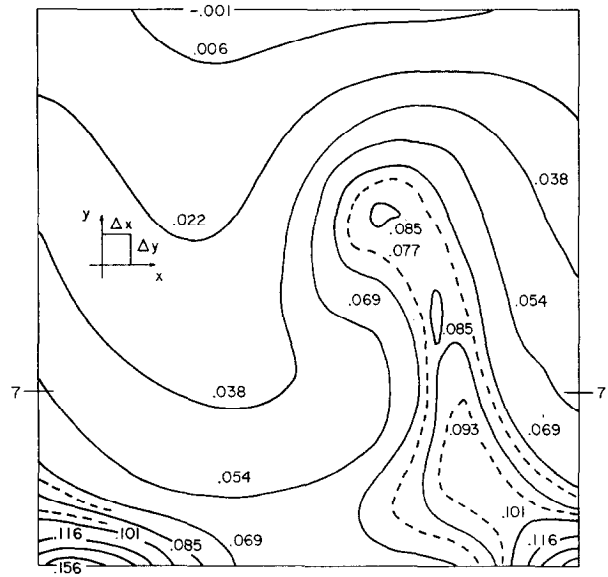

FIG. 3. Same as Fig. 2, except for run 4, convective adjustment and filter.

The presence of two-grid interval waves can be seen in run 2 (Fig. 2), oriented both east–west and north–south, especially near the southern boundary. Values of b are presented at a few gridpoints near the southernmost and northernmost rows where contours would be impractical to draw. The addition of the filter in run 4 (Fig. 3) is seen to remove the high wavenumber components near the walls, yet to leave virtually untouched the larger scale buoyancy pattern.

Along the southernmost row, values of b range from 0.316 to -0.077 in Fig. 2 and from 0.156 to 0.061 in Fig. 3. Initially, the value was 0.106; evidently some boundary problem still remains as a spuriously warm region is created even with strong filtering near the walls.

Figures 4 and 5 present east–west vertical cross sections along row $j = 7$ for levels $k = 1$ to $k = 3$. (Row $j = 7$ is located about one-third of the distance between the southern and northern walls.) Buoyancy b and vertical motion w are displayed for timestep 200; in reality, w is located $\frac{1}{2}\Delta y$ north of b but has been drawn in the same cross section. Fig. 4 displays run 2 and Fig. 5 displays run 4. We see that, except for the presence of slightly more high wavenumber components in w in the nonfiltered run, the fields are quire similar. In particular, the location

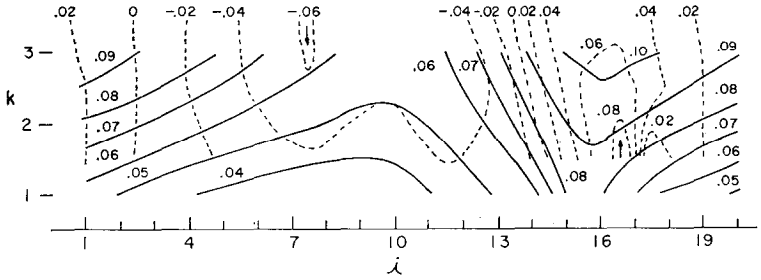

FIG. 4. Buoyancy b (solid lines), and vertical motion w (dashed lines), in $x - z$ cross section (east–west); $j = 7$, $k = 1 - 3$ for run 2, timestep 200. Tic marks show location of b gridpoints. This cross section is located between 7's in Fig. 2.

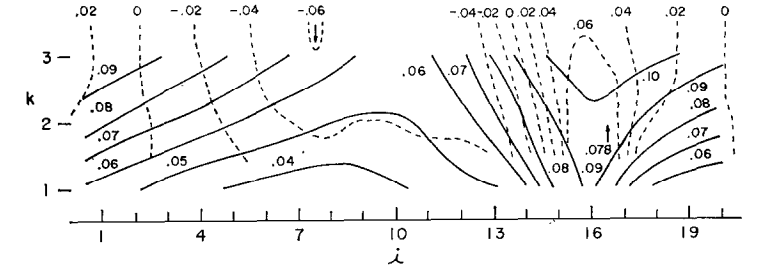

FIG. 5. Same as Fig. 4, except for run 4. Cross section is located between 7's in Fig. 3.

of the sloping cold frontal zone (between $i = 13$ and $i = 16$) and the strength of the vertical circulation around the zone are quite similar.

We next take three east–west rows of data, $b\ (i, j = 1, k = 1)$, $b(i, j = 7, k = 1)$, and $b\ (i, j = 13, k = 1)$, and we decompose the data into their Fourier components, comparing runs 2 and 4. Fig. 6 displays the amplitude versus wavenumber for each component. Timesteps 40, 120, and 200 are displayed. For row $j = 1$, just outside the southern boundary, we see from Fig. 6a that by step 200 the nonfiltered run 2 has generated nearly equal amplitudes for all wavenumbers, a fact apparent from Fig. 2. This "white noise" is to be constrasted to the behavior of run 4 where the strong filtering inside and near the wall has produced a rapid fall-off in amplitude with increasing wavenumber.

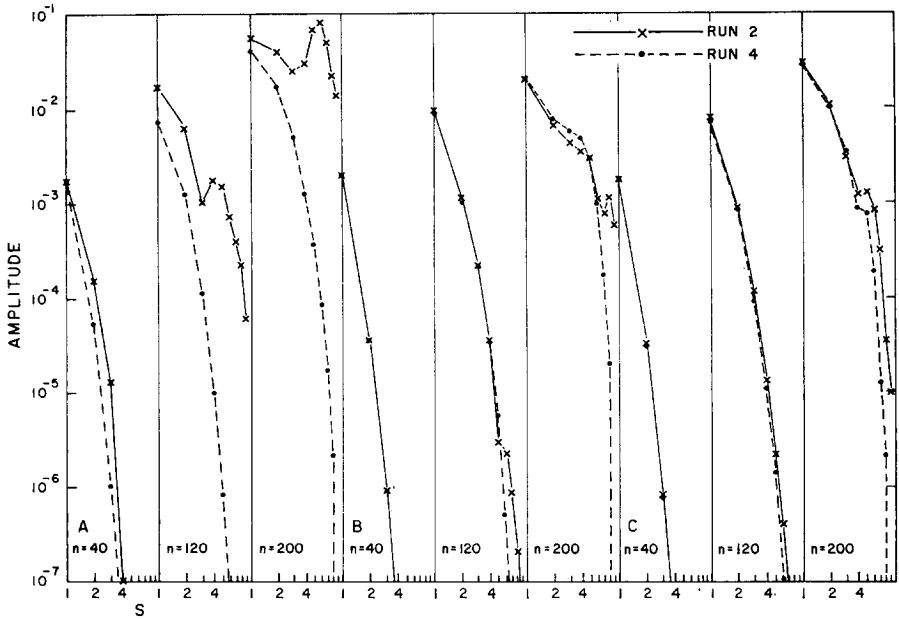

FIG. 6. Amplitude versus wavenumber S for buoyancy. Run 2 (x's and solid lines) and run 4 (dots and dashed lines). Timesteps 40, 120, and 200 are shown. A, $b(i, 1, 1)$; B, $b(i, 7, 1)$; C, $b\ (i, 13, 1)$.

Rows $j = 7$ and $j = 13$ are located in the interior, away from the strong damping near the walls. Figs. 6b and 6c show that the filter produces little change in amplitude out to wavenumber five or so, whereas higher wavenumbers are greatly reduced in amplitude. The filter completely removes the two-grid interval wave (number nine) both near the wall ($j = 1$) and in the interior ($j = 7$ and 13).

Figure 7 presents the phase versus wavenumber for each component for b

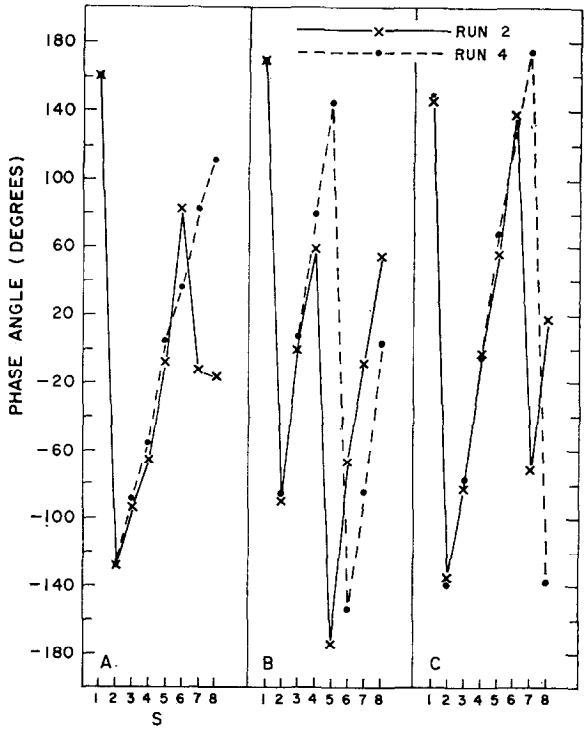

FIG. 7. Phase angle versus wavenumber S for buoyancy $b(i, 7, 1)$. Run 2 (x's and solid lines) and run 4 (dots and dashed lines). A, timestep 40; B, timestep 120; C, timestep 200.

$(i, j = 7, k = 1)$, again for timesteps 40, 120, and 200. The separation in phase between filtered and nonfiltered components is seen to be small out to wavenumbers 4 or 5.

Figures 6 and 7 thus show that, away from the boundaries, the amplitude and phase of the large-scale components are largely unchanged by the filter. Thus, Figs. 2 through 7 reveal that the filter is able to remove high wavenumber noise generated near the boundaries without significantly changing the interior, large-scale pattern, and that it is, indeed, "effective" through timestep 200.

6. DISCUSSION

For this specific initial value problem and for this specific model, the use of a scale dependent filtering technique was found to eliminate the generation of noise near the lateral boundaries. Nothing, of course, has been said concerning the

integrations beyond the time of frontal formation. The basis of the technique is the use of a strongly damping filter at the lateral walls which becomes increasingly more scale-selective with increasing distance from the walls. No attempt was made to find the "optimum" variation of the filter sensitivity with respect to distance from the walls. The crux of this problem is the need for strong damping of short waves near the boundaries, yet little filtering in the interior. In this respect, the filtering technique acts as a crude "viscous boundary layer" near the walls. As mentioned, difficulties still occur near the walls, but the integration can proceed largely independent of their effect.

Run 4 was integrated out to 800 timesteps, with no indication at that time of any impending problems. Between timesteps 220 and 480, during which time the frontal zone was dissipated, the boundary difficulties caused a spurious decrease of buoyancy near the walls, increasing the total potential energy and hence the total energy. After timestep 500, a more or less "steady state" situation was reached with one large rotating eddy located away from the boundaries. As we have no independent integration for comparison after timestep 200, we cannot conclude much about the filter's effectiveness beyond that time, except to note that it kept the interior flow uncoupled from boundary effects. The filter apparently dissipated the frontal zone, a small scale phenomenon, while having little effect on the larger scale vortex which formed from the original perturbation and which produced the frontogenesis.

APPENDIX 1: Model Conservation Criteria

The set of continuous equations conserves the total volume integrals of the momentum u, buoyancy b, energy $\frac{1}{2}(u^2 + v^2) - zb$, and potential vorticity

$$\left(\frac{\partial v}{\partial x} - \frac{\partial u}{\partial y} + f\right)\frac{\partial b}{\partial z} + \frac{\partial u}{\partial z}\frac{\partial b}{\partial y} - \frac{\partial v}{\partial z}\frac{\partial b}{\partial x}.$$

The model equations, finite-differenced in the vertical only and written in "flux" form, and in the absence of the convective adjustment scheme, conserve the total momentum M, buoyancy B, and energy E, defined as follows:

$$M = \int u_k \, dV$$

$$B = \int b_k \, dV$$

$$E = \int \left[\frac{1}{2}(u_k^2 + v_k^2) - \frac{(2k-1)}{2K} b_k\right] dV$$

where $\int dV \equiv l^{-1} \int_0^l \int_0^1 \sum_{k=1}^K \Delta z \, dy \, dx$, l is the channel length and K is the number of levels in the model ($\Delta z = K^{-1}$). No finite-difference analogue of the potential vorticity has been found to be conserved.

Consider the actual integrations, labeled runs 1 to 4. Run 1 is performed without convective adjustment and without filtering. Momentum and buoyancy are conserved to 10 decimal places while energy increases slightly with time, even before the onset of short wavelength components on the lateral boundaries. This may be due to the fact, pointed out by Williamson [11], that the Lax–Wendroff scheme is slightly unstable, both for very long and for very short wavelengths, for an equation with advection and Coriolis-type terms included. As the short wavelength components increase in amplitude, E increases more rapidly. We see from Table II that E has increased by only 1 % after timestep 160 but by over 19 % by step 220, shortly after which the run blew up. These results were repeated using a smaller timestep, ruling out linear computational instability.

Inclusion of the convective adjustment scheme causes B to decrease with time once adjustment commences. The scheme models the action of dry, turbulent convection and as such transports buoyancy upward within a column. Thus, the "center of mass of the buoyancy" $\bar{z}$, where

$$\bar{z} = \sum_{k=1}^{K} z_k b_k \Big/ \sum_{k=1}^{K} b_k$$

is increased. For this model the potential energy at a point is given by $-zb$; since the potential energy within a column is required to be conserved during adjustment, the average value of b for the column must decrease. Run 2, with convective adjustment and without filtering, shows a small decrease in B of 0.77 % by step 220. Table II also shows that M remains unchanged and E increases similarly to run 1.

The addition of the filter without convective adjustment (run 3) produces a decrease in E with time while M and B remain virtually unchanged. The addition of convective adjustment (run 4) again causes B to decrease with time; a small loss in B of 0.24 % has occurred by step 220, while E and M behave quite similarly to run 3. The increasingly rapid loss of E with time in the filtered runs demonstrates the dissipative effect of the filter. The "energy cascade" that characterizes frontogenesis shifts more and more energy to higher wavenumbers, which are damped by the filter. In addition, energy is lost near the lateral boundaries where the filter is more strongly damping at lower wavenumbers.

APPENDIX 2: LATERAL BOUNDARY CONDITION FOR b_{i1k}

The procedure used to obtain b_{i1k} is complicated by the fact that b_{ijk} and u_{ijk} are located at the same value of z. The finite-difference thermal wind relation becomes

$$\frac{1}{\Delta y}\left(\frac{1}{2}(b_{i2k}+b_{i2k-1})-\frac{1}{2}(b_{i1k}+b_{i1k-1})\right)=-f_{j=1}\frac{1}{\Delta z}(u_{i1k}-u_{i1k-1}),\qquad k=2,\ldots,K$$

for a K level model. The values of u_{i1k}, u_{i1k-1}, b_{i2k}, and b_{i2k-1} are known. The values of b_{i1k} and b_{i1k-1} are desired. We thus have K unknowns and $K-1$ equations. An additional constraint therefore is supplied; a least-squares procedure minimizing

$$\sum_{k=2}^{K}[b_{i1k}-b_{i2k}-(b_{i1k-1}-b_{i2k-1})]^2$$

allows one to find b_{i11} and, hence, all b_{i1k}'s. This constraint tends to equalize $\Delta b/\Delta y$ at all vertical levels on the $y=0$ boundary.

ACKNOWLEDGMENTS

The basic model was designed by N. Phillips and was used by the author as part of his Doctoral Research at the Massachusetts Institute of Technology. The research herein was made possible by the generous assistance of R. Shapiro, the author's branch chief, and through fruitful discussions with other colleagues.

REFERENCES

1. J. DEROME AND C. L. DOLPH, *Geophys. Fl. Dyn.* **1** (1970), 91.
2. T. GAL-CHEN AND R. C. J. SOMERVILLE, *J. Comp. Phys.* **17** (1975), 209.
3. B. G. HUNT, *Mon. Weather Rev.* **102** (1974), 3.
4. S. MANABE *et al.*, *Mon. Weather Rev.* **93** (1965), 769.
5. S. E. MUDRICK, "A Numerical Study of Frontogenesis," Thesis, Massachusetts Institute of Technology, 1973.
6. S. E. MUDRICK, *J. Atmos. Sci.* **31** (1974), 869.
7. N. A. PHILLIPS, Numerical Integration of the Hydrostatic System of Equations with a Modified Version of the Eliassen Finite-Difference Grid, *in* "Proceedings of the International Symposium on Numerical Weather Prediction, Tokyo, 1960," pp. 109–120, Meteor. Soc., Tokyo, Japan, 1960.
8. R. SHAPIRO, *Rev. Geophys. Space Phys.* **8** (1970), 359.
9. R. SHAPIRO, *J. Atmos. Sci.* **28** (1971), 523.
10. R. SHAPIRO, *Mathematics of Computation*, in press.
11. D. WILLIAMSON, *J. Comp. Phys.* **1** (1966), 51.